Physics of the Earth and Planetary Interiors 309 (2020) 106568

Contents lists available at ScienceDirect

Physics of the Earth and Planetary Interiors

journal homepage: www.elsevier.com/locate/pepi

Seismic attenuation in partially molten rocks

José M. Carcione[a,b], Biancamaria Farina[a,*], Flavio Poletto[a], Ayman N. Qadrouh[c], Wei Cheng[b]

[a] National Institute of Oceanography and Applied Geophysics - OGS, Italy
[b] School of Earth Sciences and Engineering, Hohai University, Nanjing 211100, China
[c] KACST, PO Box 6086, Riyadh 11442, Saudi Arabia

ARTICLE INFO

Keywords:
Seismic velocity
Seismic attenuation
Arrhenius equation
Grain boundary relaxation
CPA model
Hill average
Walsh model
Gassmann equation
Hashin-Shtrikman average

ABSTRACT

We compare viscoelastic models to obtain the seismic properties of a partially molten rock as a function of temperature, pressure and tectonic stress. Invoking the correspondence principle, the material of the inclusions is represented by a Maxwell mechanical model, where the Arrhenius equation and the octahedral stress criterion define the Maxwell viscosity. One of the most advanced models is the self-consistent or coherent-potential approximation (CPA), which considers oblate spheroidal inclusions of arbitrary aspect ratio and high concentration. The physical mechanism behind the Arrhenius equation is grain-boundary relaxation, and melt occurs beyond a critical temperature. The seismic properties (stiffness, wave velocity and dissipation factor) are obtained with the CPA, Hill, Hashin-Shtrikman, Walsh and Krief-Gassmann equations. The latter model and the Hashin-Shtrikman average make no assumption on the shape of the inclusions. All the models show similar trends, predicting relaxation peaks at seismic frequencies and at the brittle-ductile transition.

1. Introduction

Geophysical methodologies such as seismic surveys, processed with traveltime tomography and waveform inversion, are extensively used to map the structure of the Earth mantle and crust and understand their complex tectonic history (e.g., Finetti, 2005). The presence of partial melt gives information about this structure and the in-situ pressure-temperature conditions of rocks. Then, modeling the effects of melting on the seismic properties, particularly on anelasticity and wave attenuation, is essential (McCarthy and Takei, 2011; Jackson, 2015; Takei, 2017; Lee et al., 2017).

Partial melt occurs in the crust and mantle and plays a role to define the brittle-ductile transition and the low velocity zone in the upper mantle (Nur, 1971; Rimas Vayšnis, 1968; Anderson, 1970; Takeuchi, 1972; Jackson et al., 2006; Lee et al., 2017; Farina et al., 2019). Experiments show that melting occurs as thin lenses with low aspect ratio (ideally represented by penny shaped inclusions) and thin films wetting the rock grains (Waff and Bulau, 1979; Schmeling, 1985). Molten rocks show a high degree of attenuation, which is also relevant to characterize the seismic response of volcanoes. The squirt-flow model has been used to explain attenuation in the asthenosphere (Mavko and Nur, 1975). However, Hammond and Humphreys (2000) conclude that melt squirt is not responsible for attenuation in the seismic band, on the basis that no relaxation occurs due to fluid flow between inclusions due to pressure gradients. Thus, melt mobility has little effect on attenuation. They state: "Some conceivable melt distributions, however, would result in detectable attenuation in the seismic band".

Walsh (1968, 1969) developed a theory to obtain the seismic properties of a partial molten rock, where the stiffness of the inclusions (penny shaped cracks, Fig. 1) are represented by a Maxwell mechanical model (e.g., Karato and Spetzler, 1990; Pichler and Lackner, 2009; Carcione, 2014). Anderson (1970), Takeuchi (1972) and Schmeling (1985) have used Walsh theory to describe the seismic properties of media with partial melting. A more realistic model, not restricted to diluted inclusions, is the coherent-potential approximation (CPA) proposed by Berryman (1980a, 1980b). This approach is a self-consistent approximation and can be considered an extension of the Walsh theory and the well-known theory of Kuster and Toksóz (1974) to arbitrary volume fractions of the constituents (Berryman, 1995). This model (and Walsh's) has a parameter with the aspect ratio, a, of the inclusions, which here are assumed to be penny shaped (Fig. 1). This theory has no restriction on the melt concentration, while it takes into account the interaction between inclusions. Moreover, triple grain junctions (or grain contacts), where melt occurs, can be seen as three very thin cracks at random orientations (the three divergent boundaries ideally meet at near 120°) (Hammond and Humphreys, 2000), so that our models, based on inclusions, can be a good approximation, since at the scale of the signal wavelength, they describe effective properties in an isotropic medium.

* Corresponding author.
E-mail addresses: jcarcione@inogs.it (J.M. Carcione), bfarina@inogs.it (B. Farina).

https://doi.org/10.1016/j.pepi.2020.106568
Received 27 January 2020; Received in revised form 26 June 2020; Accepted 8 August 2020
Available online 17 September 2020
0031-9201/

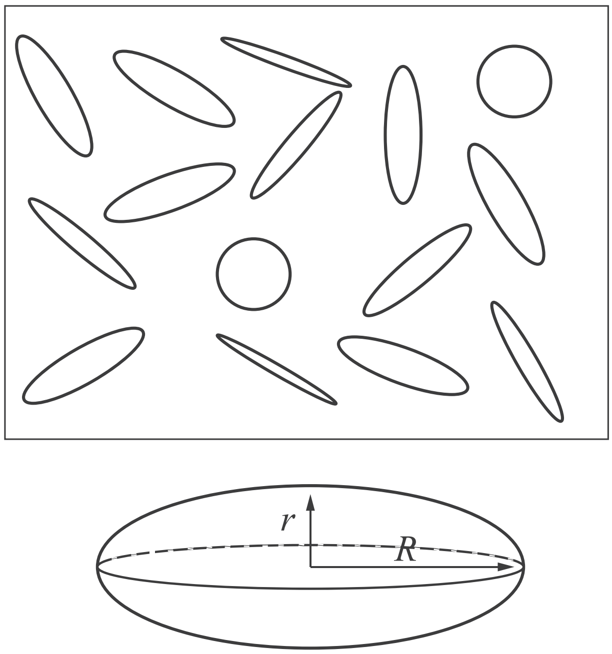

Fig. 1. Randomly oriented spherical and oblate spheroidal inclusions. The aspect ratio of the spheroidal inclusions is $a = r/R$, where the two major semiaxes of the ellipsoid are equal to R. The spheroids may represent thin films (disks), penny shaped inclusions or compliant cracks filled with molten materials between grain contacts.

Gassmann's equations are also considered (e.g., Carcione, 2014; Kim et al., 2019), based on Krief dry-rock moduli and a solid infill (the inclusions, i.e., the molten material). In this case, there is no assumption on the shape of the inclusions. Gassmann's equation generalized to the case of a solid pore infill has been introduced by Ciz and Shapiro (2007) and Carcione et al. (2011). Moreover, a composite medium has stiffness bounds given by the Hashin-Shtrikmann-Walpole (HS) equations (e.g., Mavko et al., 2009), which provide a range of validity, since these bounds hold by any geometrical configuration of the two-phase composite. The averages of these bound generally provide a suitable estimate of the stiffnesses.

The properties of the partially molten medium (frame and inclusion) depend on stress and temperature through the Maxwell shear viscosity (e.g., Walsh, 1969; Pichler and Lackner, 2009; Carcione and Poletto, 2013; Carcione et al., 2014; Carcione et al., 2017). We perform a comparative analysis of the different models, namely, the simple and heuristic Voigt-Reuss-Hill average, the HS average, Gassmann equations, Walsh model and the CPA model. All the models consider an isotropic frame and the last two are based on oblate spheroidal inclusions. We combine these models with the Arrhenius equation, based on the octahedral stress criterion, including the effect of temperature (e.g., Carcione et al., 2006; Carcione and Poletto, 2013) to obtain the seismic properties as a function of depth.

2. Models of effective stiffness moduli

We assume a background medium composed of n phases with randomly oriented and ellipsoidal isolated inclusions of bulk and shear moduli K_i and μ_i, $i = 1, \ldots, n$, where 1 and $2, \ldots, n$ refer to the background (frame) and inclusions, respectively. We consider five models to obtain the stiffnesses of the composite, where the inclusions have a minor axis to major axis ratio (the aspect ratio) ranging from $a = 1$ (stiff pores) to $a \ll 1$ (cracks). The molten (or partially molten) phases have the form of oblate spheroids (Fig. 1).

2.1. Arrhenius viscosity related to grain-boundary relaxation

The shear modulus of the frame and inclusions are mechanically represented by the Maxwell model, i.e.,

$$\mu_i = G_i\left(1 - \frac{\mathrm{i}G_i}{\omega\eta_i}\right)^{-1} \tag{1}$$

where G_i is the rigidity at infinite frequency and infinite viscosity, η_i is the Maxwell viscosity, ω is the angular frequency, and $\mathrm{i} = \sqrt{-1}$ (e.g., Carcione, 2014). For $\eta_i \to 0$, $\mu_i \to 0$ and the medium becomes a fluid.

The viscosity η_i can be expressed by the Arrhenius equation (Carcione and Poletto, 2013) as

$$\eta_i = \frac{\sigma_o^{1-n_i}}{2A_i}\exp(E_i/RT), \tag{2}$$

where σ_o is the octahedral stress,

$$\sigma_o = \frac{1}{3}\sqrt{(\sigma_v - \sigma_h)^2 + (\sigma_v - \sigma_H)^2 + (\sigma_h - \sigma_H)^2} \tag{3}$$

(e.g., Carcione et al., 2006), where σ is the stress component in the principal system, corresponding to the vertical (v) lithostatic stress, and the maximum (H) and minimum (h) horizontal tectonic stresses, A_i and n_i are constants, E_i is the activation energy, $R = 8.3144$ J/mol/°K is the gas constant and T is the absolute temperature. The form of the relation (2) is determined by performing experiments at different strain rates, temperatures and/or stresses (e.g., Gangi, 1983). The physical mechanism behind the Arrhenius equation is grain-boundary relaxation. Rocks can be viewed as composites of crystalline particles or "grains" separated by thin amorphous grain boundaries. The disaggregation of these boundaries induces anelasticity. This process takes places continuously before melting (e.g., Zhang et al., 2009; Takei, 2017). We have applied this model from 2013 (Carcione et al., 2018b and references therein), where we have combined viscoelasticity and poroelasticity with the Arrhenius equation. Fig. 5 in Carcione and Poletto (2013, Eq. (24)) shows that the velocities and quality factors abruptly decrease after a given viscosity dictated by a critical (transition) temperature and the Arrhenius equation. This quantity is analogous to the solidus temperature in Takei (2017).

2.2. Voigt-Reuss-Hill average

The Reuss and Voigt bounds are the wider bounds possible. The average is termed Voigt-Reuss-Hill (VRH) average. The Voigt (K_V) and Reuss (K_R) averages are iso-strain and iso-stress approximations, respectively (the stress and strain are unknown and are expected to be non-uniform). Despite its simplicity, the VRH estimates were found in most cases to have an accuracy comparable to those obtained by more sophisticated techniques such as self-consistent schemes and are valid for complex rheologies such as general anisotropy and arbitrary grain topologies (e.g., Man and Huang, 2011; Picotti et al., 2018). For two phases of proportions $1 - \phi$ and ϕ (inclusions), the composite bulk modulus is

$$K = \frac{1}{2}(K_V + K_R), \tag{4}$$

where

$$K_V = (1-\phi)K_1 + \phi K_2 \text{ and } K_R^{-1} = (1-\phi)K_1^{-1} + \phi K_2^{-1}, \tag{5}$$

and a similar equation for μ, replacing K_i with μ_i, $i = 1, 2$.

2.3. Hashin-Shtrikman average

It is well known that an elastic two-phase composite, with no restriction on the shape of the two phases, has stiffness bounds given by the Hashin and Shtrikman (1963) equations,

$$K_{\rm HS}^{\pm} = K_1 + \frac{\phi}{(K_2 - K_1)^{-1} + (1-\phi)\left(K_1 + \frac{4}{3}\mu_\beta\right)^{-1}} \tag{6}$$

and

$$\mu_{\rm HS}^{\pm} = \mu_1 + \frac{\phi}{(\mu_2 - \mu_1)^{-1} + (1-\phi)\left[\mu_1 + \frac{\mu_\beta}{6}\left(\frac{9K_\beta + 8\mu_\beta}{K_\beta + 2\mu_\beta}\right)\right]^{-1}}, \tag{7}$$

where we obtain the upper bounds when K_β and μ_β are the maximum bulk and shear moduli of the single components, and the lower bounds when these quantities are the corresponding minimum moduli, i.e., if $\beta = 1$ (stiffer medium), we have the upper bounds, and $\beta = 2$ gives the lower bounds (Mavko et al., 2009).

The averages of these bounds are

$$K = \frac{1}{2}(K_{\rm HS}^{+} + K_{\rm HS}^{-}),\quad \mu = \frac{1}{2}(\mu_{\rm HS}^{+} + \mu_{\rm HS}^{-}). \tag{8}$$

Then, the model parameters in this case are the melt proportion, ϕ, and the stiffnesses of the background and molten phase, where the shear moduli can be complex.

2.4. Walsh model

In this model, the stiffness of the inclusions (penny shaped) are represented by a Maxwell mechanical model. Walsh neglects the interaction between the inclusions and this requires a dilute solution, i.e., the porosity must be less or equal to the aspect ratio of the inclusions [Walsh removed the self-consistent assumption present in Wu (1966)].

The effective bulk modulus K and effective rigidity μ are (Walsh, 1969),

$$\frac{K_1}{K} - 1 = \phi\left(1 - \frac{K_2}{K_1}\right)\frac{3K_1 + 4\mu_2}{3K_2 + 4\mu_2 + \gamma} \tag{9}$$

and

$$\frac{\mu_1}{\mu} - 1 = \frac{\phi}{5}\left(1 - \frac{\mu_2}{\mu_1}\right)\left[1 + \frac{8\mu_1}{4\mu_2 + \gamma_1} + \frac{2(3K_2 + 2\mu_2 + 2\mu_1)}{3K_2 + 4\mu_2 + \gamma}\right], \tag{10}$$

where

$$\gamma = \frac{3\pi a\mu_1(3K_1 + \mu_1)}{3K_1 + 4\mu_1},\quad \gamma_1 = \frac{3\pi a\mu_1(3K_1 + 2\mu_1)}{3K_1 + 4\mu_1}, \tag{11}$$

and ϕ is the concentration of the inclusions, which is assumed to be very small in this model, i.e., $\phi \ll 1$. Strictly, we obtain the Walsh model for $\eta_1 = 0$ and $G_2 = 0$. The theory holds for $a \ll 1$. In this case, an additional parameter is the aspect ratio, a.

2.5. Gassmann model

The poroelasticity theory provides other expressions, based on Gassmann equations. Since we are dealing with molten material, we use the generalization of these equations to the case of a solid pore-infill, obtained by Ciz and Shapiro (2007). In this way, we can model, partial melting, i.e., melt and fluid in the pore space. The Gassmann moduli are

$$K = \frac{K_1 - K_m + \phi K_m(K_1/K_2 - 1)}{1 - \phi - K_m/K_1 + \phi K_1/K_2},\quad K_m = K_1(1-\phi)^{\Lambda/(1-\phi)} \tag{12}$$

and

$$\mu = \frac{\mu_1 - \mu_m + \phi\mu_m(\mu_1/\mu_2 - 1)}{1 - \phi - \mu_m/\mu_1 + \phi\mu_1/\mu_2},\quad \mu_m = \mu_1(1-\phi)^{\Lambda/(1-\phi)}, \tag{13}$$

where K_m and μ_m denote the dry-rock moduli obtained with Krief equation (Carcione et al., 2011), where Λ is a lithological parameter, which is related to the degree of compaction versus depth. These equations are approximate and may violate the bounds when exceeding a critical porosity value of 0.4 approximately. This happens because the Gassmann moduli approach the Reuss bound and the isostress assumption behind this bound does not apply for isotropic composites made of solids, i.e., when each component has a finite shear modulus. In this case, the model parameters are the melt proportion, ϕ, the stiffnesses of the background and molten phase, and Λ in Krief equations. Here, we consider $\Lambda = 12$.

2.6. Self-consistent scheme (CPA model)

In the self-consistent approximation, the interaction of inclusions is approximated by replacing the background medium with an unknown effective medium whose stiffnesses have to be found implicitly. The CPA model has been used by Gurevich and Carcione (2000) to obtain the stiffnesses of sand-clay mixtures, where the inclusions are spherical, i.e., $a = 1$. In the CPA scheme, the effective bulk and shear moduli of a composite medium (K and μ), with n spheroidal inclusions, each with aspect ratio a_i and proportion ϕ_i, are obtained as the roots of the following system of equations

$$\sum_{i=1}^{n}\phi_i(K_i - K)P_i = 0,\qquad \sum_{i=1}^{n}\phi_i\left(\mu_i - \mu\right)Q_i = 0, \tag{14}$$

for n phases, where

$$P_i = \frac{K + \frac{4}{3}\mu_i}{K_i + \frac{4}{3}\mu_i + \pi a_i\beta},\quad i = 1,\dots,n$$
$$Q_i = \frac{1}{5}\left[1 + \frac{8\mu}{4\mu_i + \pi a_i(\mu + 2\beta)} + 2\frac{K_i + \frac{2}{3}(\mu_i + \mu)}{K_i + \frac{4}{3}\mu_i + \pi a_i\beta}\right],$$
$$\beta = \mu\frac{3K + \mu}{3K + 4\mu} \tag{15}$$

for penny-shaped cracks ($a_i \ll 1$) and

$$P_i = \frac{K + \frac{4}{3}\mu}{K_i + \frac{4}{3}\mu},\quad i = 1,\dots,n$$
$$Q_i = \frac{\mu + \zeta}{\mu_i + \zeta},$$
$$\zeta = \frac{\mu}{6}\cdot\frac{9K + 8\mu}{K + 2\mu} \tag{16}$$

for spheres (Berryman, 1980a, 1980b, 1995; Mavko et al., 2009, p. 187),

For two phases, we have

$$(1-\phi)(K_1 - K)P_1 + \phi(K_2 - K)P_2 = 0,\qquad (1-\phi)(\mu_1 - \mu)Q_1 + \phi(\mu_2 - \mu)Q_2 = 0. \tag{17}$$

A limitation of this theory is that the inclusions are isolated, so that pore pressures are not equilibrated. The expressions for penny-shaped cracks hold for soft inclusions (compared to the background) and small aspect ratios (Walsh, 1969; Berryman, 1980b). Actually, there are (more complex) exact expressions for P and Q, which hold for any aspect ratio of the oblate spheroidal inclusions, including spherical inclusions and thin cracks: $P = \frac{1}{3}T_{iijj}$ and $Q = \frac{1}{5}(T_{ijij} - P)$, where T_{iijj} and T_{ijij} are given in Appendix A of Berryman (1980b) or in page 189 of Mavko et al. (2009). The expressions P_1 and Q_1 for spherical inclusions are exact, while the approximations P_2 and Q_2 slightly deviate from the exact expressions at high aspect ratios of the cracks.

3. Seismic properties

The phase velocity, attenuation factor and quality factor are

$$c_p = \left[\mathrm{Re}\left\{\frac{1}{c}\right\}\right]^{-1}, \tag{18}$$

$$\alpha = -\omega\,\mathrm{Im}\left\{\frac{1}{c}\right\} \tag{19}$$

and

$$Q = \frac{\mathrm{Re}\{c^2\}}{\mathrm{Im}\{c^2\}}, \tag{20}$$

respectively, where $\omega = 2\pi f$ is the angular frequency, c denotes c_P or c_s, being the complex and frequency-dependent P-wave and S-wave velocities, respectively,

$$c_P = \sqrt{\frac{K + 4\mu/3}{\rho}} \text{ and } c_S = \sqrt{\frac{\mu}{\rho}}, \tag{21}$$

where ρ is the bulk mass density (Mainardi, 2010; Carcione, 2014).

4. Results

We first consider the CPA model and the well-known example given in Mavko et al. (2009) in page 188 as a reference, and generalize it to the viscoelastic case by considering a Maxwell viscosity associated to the shear modulus of the inclusions (this viscosity is a free parameter). The CPA model is considered to be the most advanced. The problem consists in calculating the complex effective bulk and shear moduli of a rock consisting of spherical quartz grains ($a = 1$) and total porosity 0.3. The pore space consists of spherical inclusions ($a = 1$) and thin, penny-shaped cracks ($a = 0.01$). The thin cracks have a porosity of 0.01, and the remaining porosity (0.29) is made up of the spherical pores. The inclusions are modeled as in Walsh (1968, 1969), i.e., with $\mu = \mathrm{i}\omega\eta = 2\pi\mathrm{i}f\eta$, where f is the frequency. The number of phases is $n = 3$ and the medium properties are shown in Table 1. To solve Eq. (14), we use the algorithm developed by Goffe et al. (1994), based on Corana et al. (1987). The Fortran code can be found in: https://econwpa.ub.uni-muenchen.de/econ-wp/prog/papers/9406/9406001.txt. Fig. 2 shows the results. We can see two peaks with very low values of Q, at $\log_{10}(2\pi f\eta) = -0.5$ and 1.5, corresponding to $f = 0.05\,\eta^{-1}$ GPa, and $f = 5\,\eta^{-1}$ GPa, respectively. For $\eta = 10^{-3}$ GPa · s, we obtain 50 Hz and 5 kHz; and $\eta = 10$ GPa · s yields 0.005 Hz and 0.5 Hz, respectively. At high values of $\omega\eta$ the model predicts extremely high attenuation values, proper of diffusion fields, not waves.

We now consider a medium with cracks filled with a molten material. Takei (2000) provides the properties of borneol-diphenylamine at 50 °C, a binary eutectic system of the organic compounds, an appropriate analogue of melting in the Earth's mantle (Table 3 in that paper). The solid frame has $K_1 = 3.11$ GPa, $\mu_1 = 0.877$ GPa and $\rho_1 = 1011$ kg/m^3, whereas the molten material has $K_2 = 2.67$ GPa, $\mu_2 = \mathrm{i}\omega\eta$, $\rho_2 = 1051$ kg/m^3, with η a free parameter. We consider $\Lambda = 12$, $\phi = 5\%$, the aspect ratios $a_1 = 1$ and $a_2 = 0.01$, and $\eta = 0.001$ GPa · s $= 10^6$ Pa · s $= 10^7$ P. Nur (1971) inferred a range 10^6–10^{12} P for the viscosity of melt in the low-velocity zone under North America.

Figs. 3 and 4 show the P- and S-wave phase velocity (a) and

Table 1
Rock properties.

Medium	K (GPa)	μ (GPa)	ϕ	ρ (kg/m^3)
1	37	44	0.7	2650
2	2.25	$\mathrm{i}\omega\eta$	0.29	1040
3	2.25	$\mathrm{i}\omega\eta$	0.01	1040

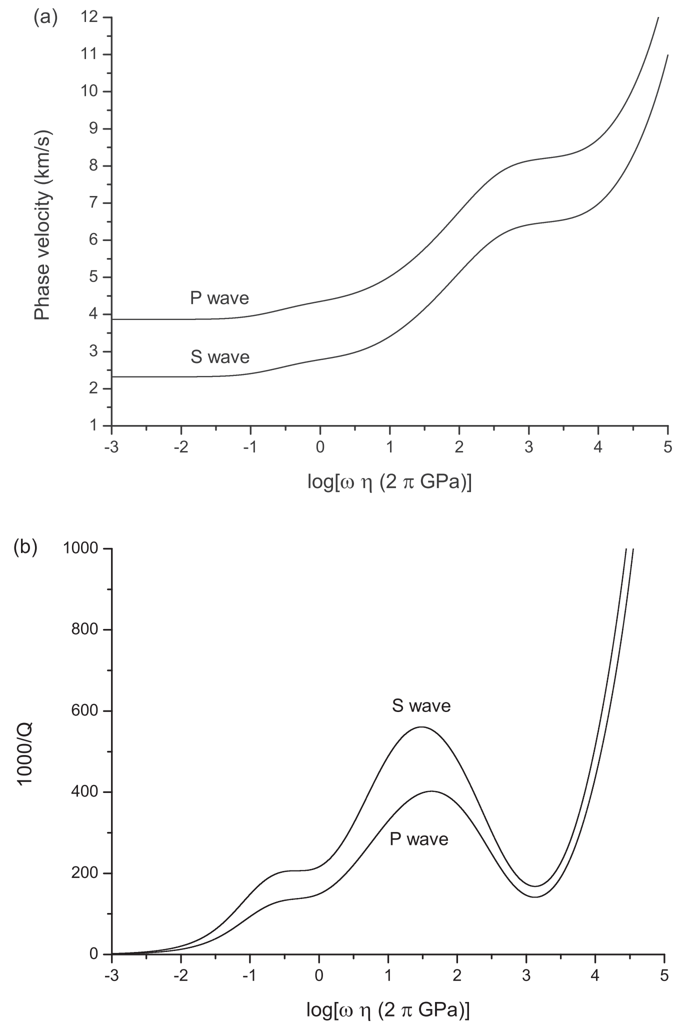

Fig. 2. Phase velocity (a) and dissipation factor (b) as a function of $\log_{10}(\omega\eta)$ corresponding to the CPA model and the generalization to the anelastic case of a problem solved in Mavko et al. (2009, p. 188).

dissipation factor (b). All the models predict a peak of the dissipation factor between 1 and 10 Hz, with similar strength ($Q_P \approx 13$ and $Q_S \approx 3$), whereas the Walsh model predicts a second strong peak at the sonic frequencies (10 KHz). The VRH, HS and CPA models predict a diffusive behavior of the P wave at high frequencies (Q_P is very low), and the slopes follow that of the Walsh peak. Gassmann model, based on a low-frequency assumption, gives a different high-frequency limit, as well as the Walsh model, which shows a negative dispersion behavior. However, in this case, all the models should be considered reliable at seismological and seismic-technology frequencies, say, up to 1 KHz. The imaginary part of the bulk modulus is negligible in all the cases, so that there is no loss due to dilatational deformations of the medium. The attenuation of the P wave is mainly due to shear deformations, such that for all the models $Q_P \approx Q_S + 0.75\,Re(K)/Im(\mu) > Q_S$. It is remarkable that all the models predict a similar loss and velocity dispersion. This confirms the fact that even simple heuristic models, such as the VRH model, are suitable from a practical point view. Fig. 5 shows the variations of the P-wave velocity and attenuation with aspect ratio. Velocities decrease with decreasing aspect ratio (Xu and Payne, 2009; Yang et al., 2017), whereas the strength of the peaks and velocity dispersion increase for decreasing aspect ratio. The second peak of the Walsh model at 10 KHz and the slope of the CPA model at high frequencies do not depend on the aspect ratio.

The Walsh and CPA models are based on isolated inclusions and no

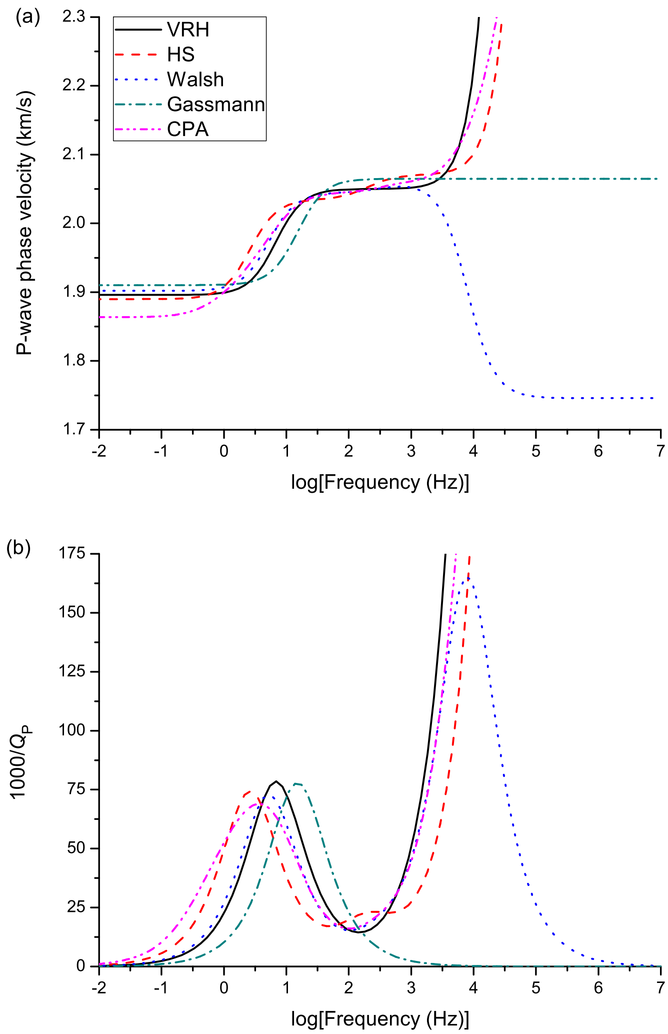

Fig. 3. P-wave phase velocity (a) and dissipation factor (b) as a function of frequency.

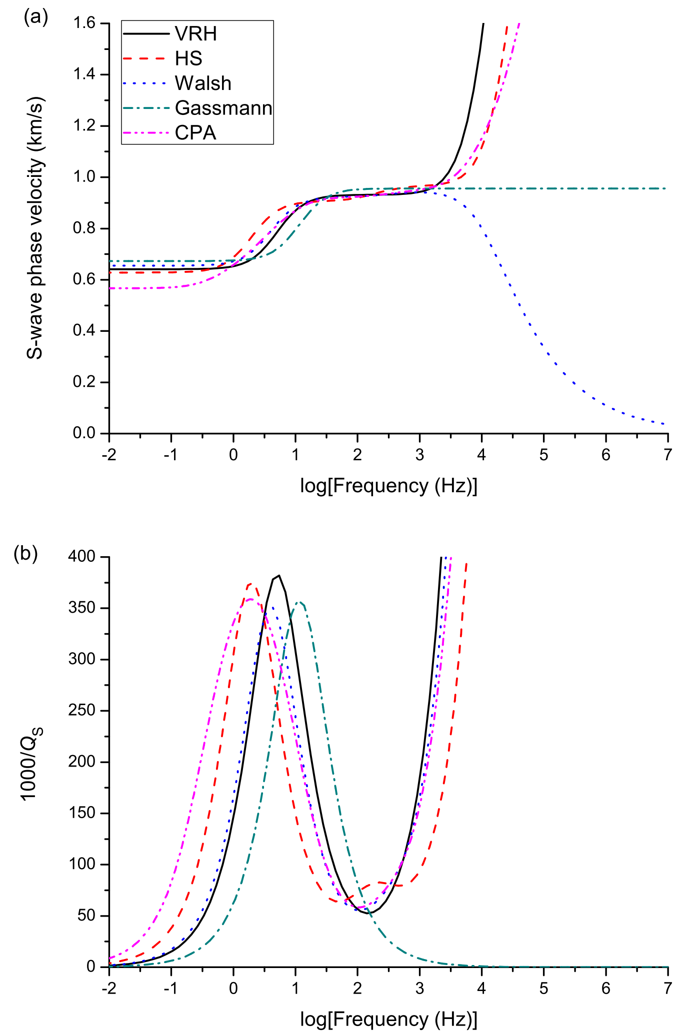

Fig. 4. S-wave phase velocity (a) and dissipation factor (b) as a function of frequency.

flow takes place, so that there is no time for wave-induced pore-pressure increments to flow and equilibrate. This behavior is appropriate to ultrasonic laboratory conditions. However, both models predict relaxation peaks at the seismic band. Walsh (1969) states that there is a low-frequency peak at $f_p \approx \delta\mu_1/\eta = 2.8$ Hz ($\log f_p = 0.45$) [$\delta = \gamma_1/(4\mu_1)$], so that if a is small and η is large enough, the critical frequency can occur in a range of geophysical interest.

We now consider the Arrhenius equation to define the shear modulus of the inclusions, with the aspect ratio varying with depth. According to Sun and Goldberg (1997a,b), the aspect ratio can be expressed with an exponential dependence on the effective pressure. Here, we consider a linear transition from a_0 to $a_\infty < a_0$, the values at the initial and final depths, respectively. The temperature is a function of depth through the geothermal gradient G as $T = zG$, where z is depth. The lithostatic stress is $\sigma_v = -\bar{\rho} g z$, where $\bar{\rho}$ is the average density and $g = 9.81$ m/s^2 is the gravity constant. To obtain the octahedral stress (3) we consider a simple model based on the gravity contribution at depth z. The horizontal stresses is estimated as $\sigma_H = \nu\sigma_v$ and $\sigma_h = \xi\sigma_H$, with $\nu = (3K_1 - 2G_1)/[2(3K_1 + G_1)]$ the Poisson ratio. The parameter $\xi \le 1$ has been introduced to model additional effects due to tectonic activity (anisotropic tectonic stress).

We consider the properties listed in Table 2 and a frequency of 3 Hz. Moreover, $a_\infty = 0.001$, $a_0 = 0.02$, $G = 60$ °C/km, $\bar{\rho} = 2600$ kg/m^3 and $\xi = 0.8$. There are two activation energies, that of the background (E_1) and that of the inclusions (E_2), the inclusions melting at a lower temperature. The above degree of stress anisotropy is consistent with values at prospective depths provided by Hegret (1987) for the Canadian Shield, and in agreement with data reported in Engelder (1993, p. 91).

Fig. 6 shows the shear-wave velocity and dissipation factor of the background and inclusions as a function of depth, where the viscosity decreases from 18 GPa · s to approximately 4×10^{-4} GPa · s. At this viscosity, the melt is almost a fluid, since the velocities approach zero with increasing depth. This is the case of mid-ocean ridge basalt (MORB) melts, that have viscosities between 10^{-10} GPa · s and 10^{-6} GPa · s (Villeneuve et al., 2008). The transition from brittle to ductile of the mineral and inclusions occurs at different depths, 9 and 11 km, respectively, due to the different activation energies of the two phases. This is a specific example where the transitions are very shallow and there may be cases where these transitions are deeper. As an average, the brittle-ductile boundary occurs between 13 and 18 km. Fig. 7 shows the velocities and dissipation factors of all the models, whose results are very similar. Similar velocity curves are reported in Lee et al. (2017, Fig. 4), but as a function of the fraction of melt. The P-wave dissipation factor has quasi-symmetric peak similar to a relaxation peak. Its location depends on the value of the activation energies, where lower activation energies imply shallower peak depths. Similar peaks at a given depth have previously been predicted by Carcione and Poletto (2013) and Carcione et al. (2018a,b) with the Burgers model. Since the properties depend on $\omega\eta_1$ and $\omega\eta_2$, the peaks move to shallow depths for

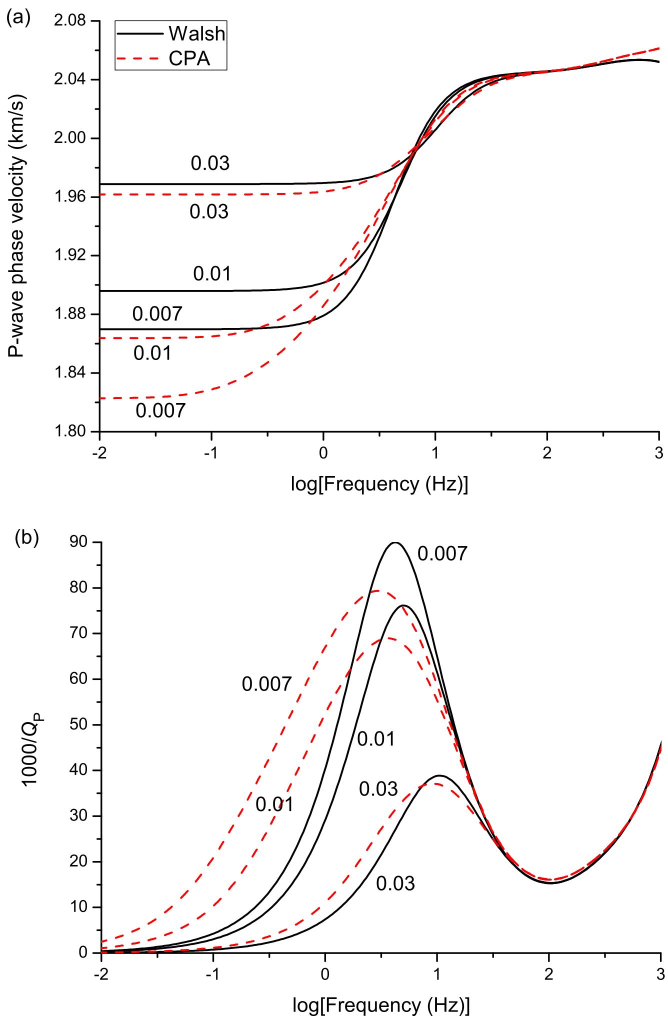

Fig. 5. P-wave phase velocity (a) and dissipation factor (b) as a function of frequency, corresponding to the Walsh and CPA models. The numbers indicate the aspect ratio.

Table 2
Rock properties.

Medium	K (GPa)	G (GPa)	ϕ	ρ (kg/m^3)	n	A (MPa)$^{-n}$s^{-1}	E kJ/mol
1	60	$3K/5$	0.95	2800	2	100	140
2	40	$3K/5$	0.05	2600	2	100	120

decreasing frequency. If we take E_2 = 90 kJ/mol, the inclusions melt at shallower depths. Fig. 8 shows that all the models clearly predict two peaks, whose locations are determined by the activation energies.

Finally, we compare the theoretical results to experimental data, although there is a lack of data in the literature regarding attenuation as a function of temperature of partial molten media. Sato et al. (1988) provides ultrasonic P-wave velocity and Q factor of peridotite versus temperature. Most of the input parameters needed for the theory are absent in this work. However, we attempt a qualitative comparison, trying to honour the conditions of the experiment as better as possible. Fig. 9 shows the experimental data, although the velocity and Q have been measured at different pressure conditions. We consider the properties given in Table 3, and f = 300 kHz, $a_0 = a_\infty$ = 0.01, σ_o = 200 MPa, and ϕ = 0.25. The theoretical results are shown in Fig. 10, corresponding to the P-wave phase velocity (a) and quality factor (b) of peridotite as a function of temperature obtained with four

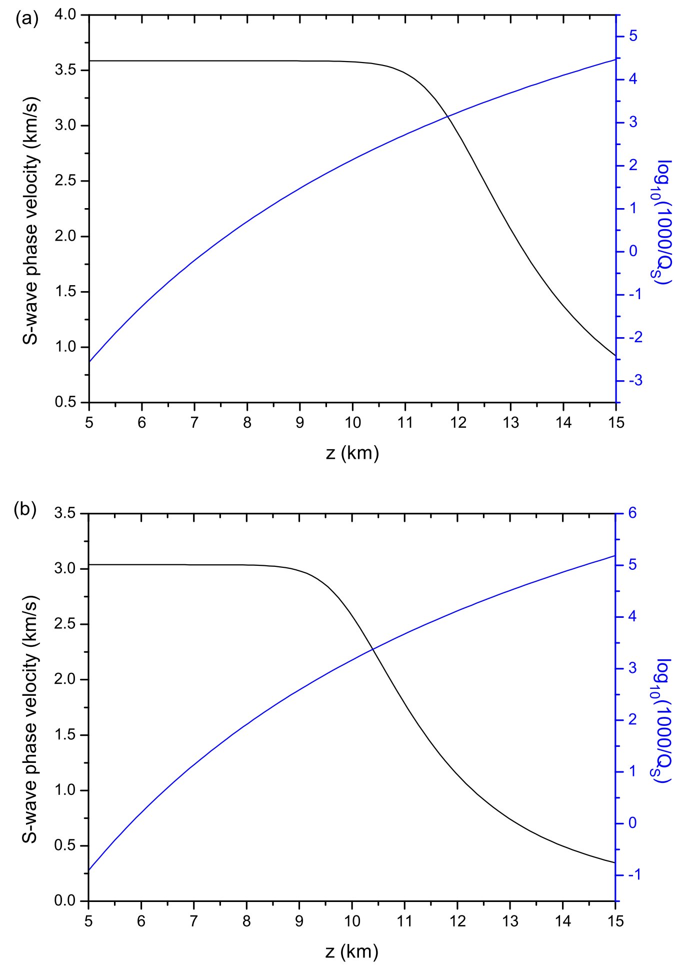

Fig. 6. S-wave phase velocity and dissipation factor of the background medium (frame) (a) and inclusion (b) as a function of depth.

different models. As can be seen, the behavior of the model predictions is qualitatively similar to the experimental data in Fig. 9.

4.1. Further research

Other models that can be applied to calculate the quality factor of molten rocks are given in Rimas Vayšnis (1968), Kerner (1956), Hill (1963, 1965) and Richard (1975), that have to be generalized to the viscoelastic case. The model by Mavko (1980) is based on pores with the geometry of tubes. Mavko found that increasing attenuation is expected when melt is in the form of films; the least where in the tube geometry; and almost any intermediate values when mixtures of tubes and films. This effect can further be studied in the context of this work.

Takei (2017) stated that geochemical studies show that the melt fraction during partial melting is small (≈0.1%), and it is difficult to explain upper-mantle low-velocity regions by the effects of melt. Takei indicates grain-boundary relaxation to induce significant polycrystal anelasticity before partial melting in the absence of melt, to be the cause of the observed attenuation.

To improve the model, pressure effects on the viscosity can be introduced, where

$$\eta = \exp[k_1(1 + k_2 p)/T], \tag{22}$$

where p is pressure and k_1 and k_2 are constants (Nur, 1971). This equation is a generalization of the Arrhenius Eq. (2). At shallow depths, the temperature effect is dominant and viscosity decreases significantly with depth. At greater depth, pressure causes the viscosity to increase.

Heat flow, neglected in this case, can be another cause of

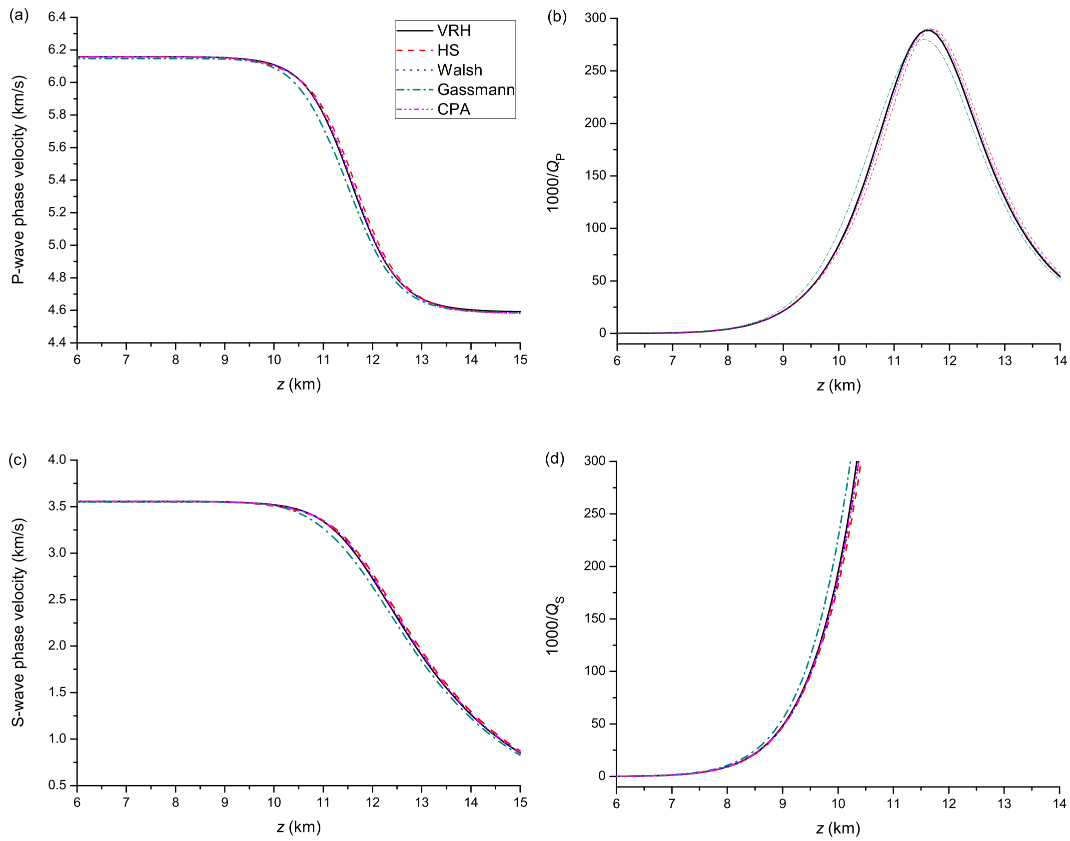

Fig. 7. P- and S-wave phase velocity (a and c) and dissipation factor (b and d) as a function of depth for activation energies of 140 and 120 kJ/mol (frame and inclusions, respectively) and a frequency of 3 Hz.

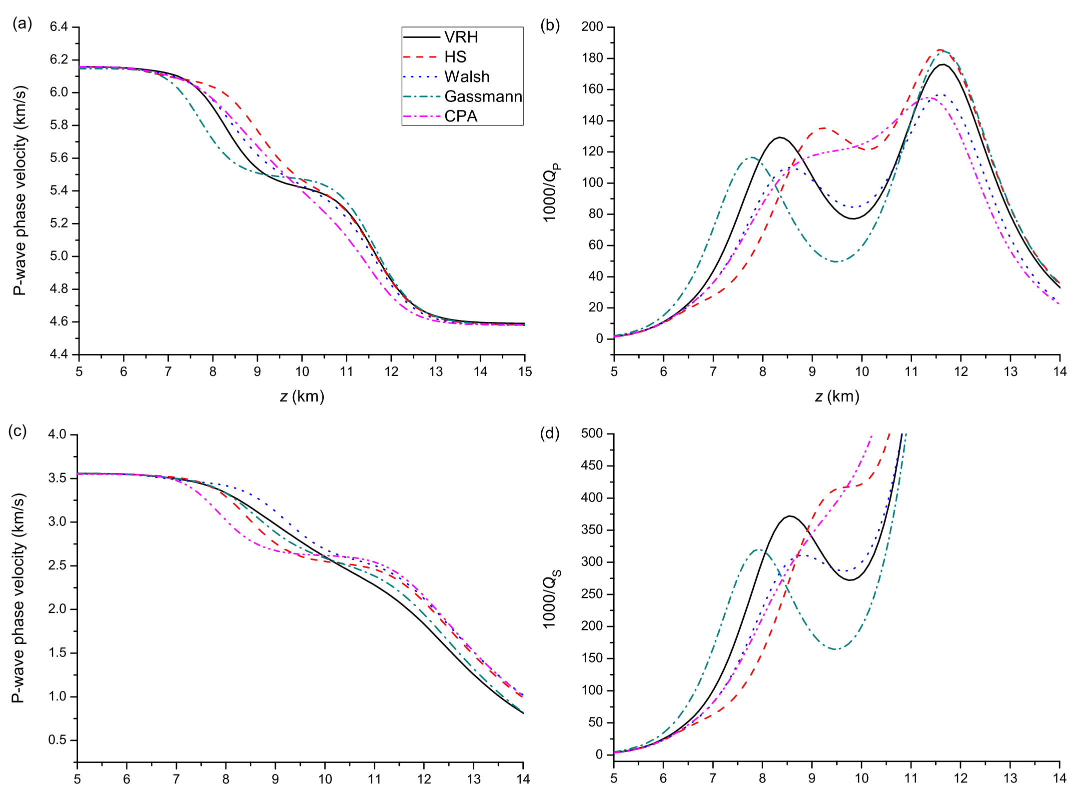

Fig. 8. P- and S-wave phase velocity (a and c) and dissipation factor (b and d) as a function of depth for activation energies of 140 and 90 kJ/mol (frame and inclusions, respectively) and a frequency of 3 Hz.

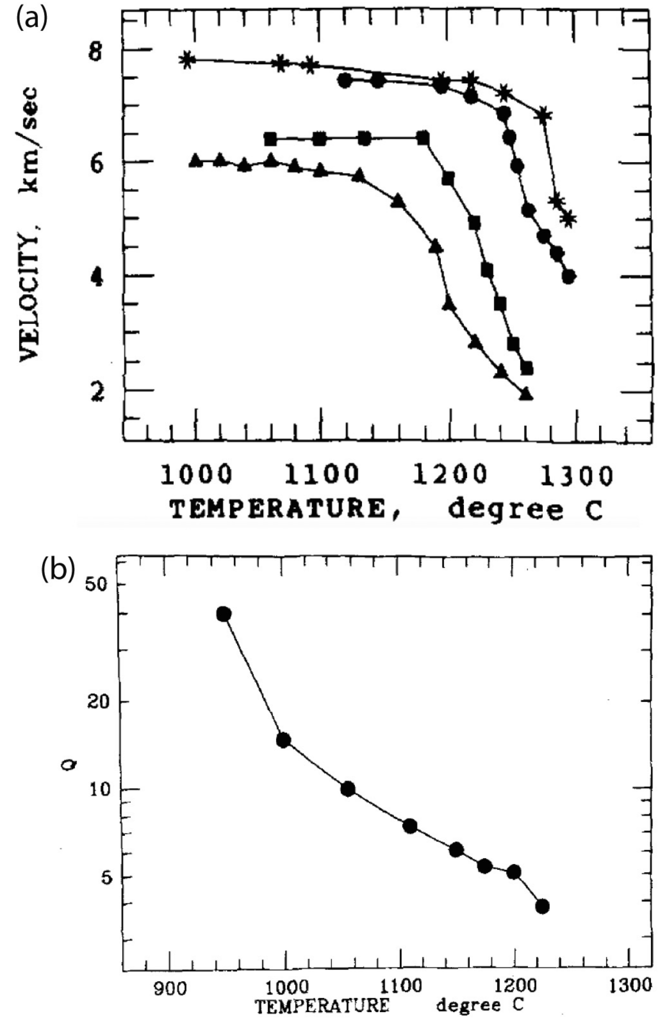

Fig. 9. Experimental data. P-wave phase velocity (a) and quality factor (b) of peridotite as a function of temperature at various pressures (after Sato et al., 1988). Here, we consider the data corresponding to the full circles.

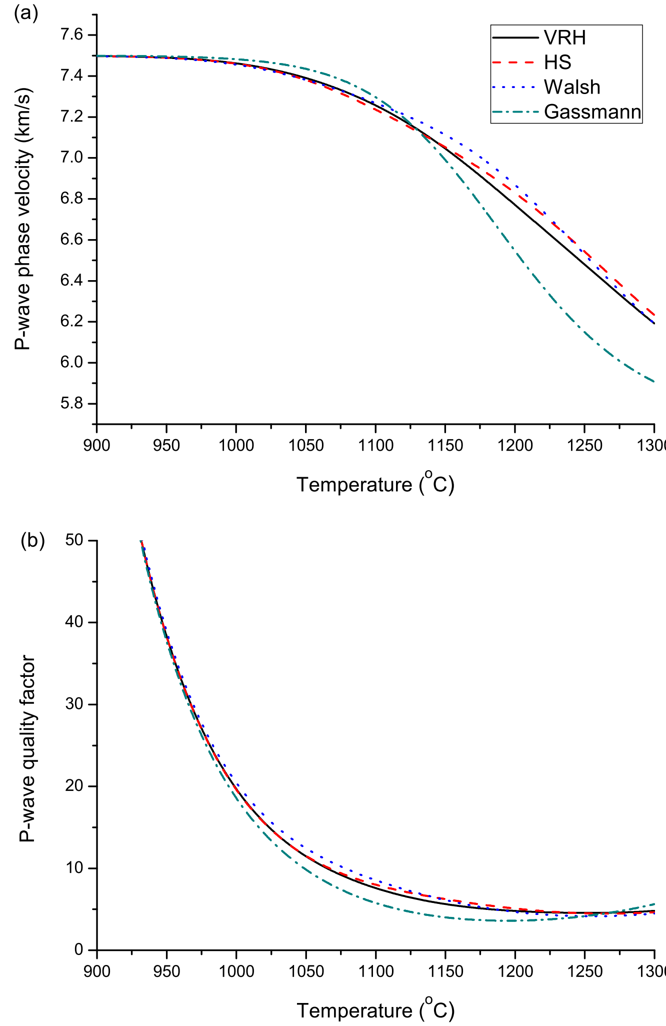

Fig. 10. P-wave phase velocity (a) and quality factor (b) of peridotite as a function of temperature obtained with four different models.

Table 3
Properties of peridotite.

Medium	K (GPa)	G (GPa)	ρ (kg/m^3)	n	A (MPa)$^{-n}$s^{-1}	E kJ/mol
1	97	54	3000	2	10^6	210
2	97	54	3000	2	10^6	180

attenuation (e.g., Carcione et al., 2018c). Adiabatic temperatures are induced, different in the solid and melt phases because of their different thermodynamic constants. One mechanism occurs when these local adiabatic temperature gradients are relaxed. A second relaxed state occurs when the induced solid-melt phase change is complete and the local temperature gradients resulting from the release or absorption of latent heat of fusion are relaxed (Mavko, 1980).

The analysis presented here can also have applications to model the properties of carbonate rocks, where the pore infill is a fluid and cracks of different aspect ratios are present. Xu and Payne (2009) considered the lossless case based on equant and soft pores. A generalization to the anisotropic case can be based on Henriques et al. (2017), with suitable anelastic properties.

5. Conclusions

We have compared viscoelastic models to obtain the seismic properties of partially molten rocks as a function of temperature, depth and pressure. The inclusions are represented by a Maxwell mechanical model, where the Arrhenius equation and the octahedral stress criterion define the Maxwell viscosity, which describes the brittle and ductile behavior of the partially molten material. All the models show similar trends, predicting relaxations peaks at seismic frequencies and as a function of depth, at the brittle-ductile transition. The self-consistent or coherent-potential approximation, which considers oblate spheroidal inclusions of arbitrary aspect ratio, can be useful to obtain information about the geometrical characteristics of the pore space. Applications range from global seismology to geothermal studies. The models can be used to improve our knowledge of partial melt in the crust and mantle. In this case, the presence of supercritical fluids can easily be implemented into the theory.

Declaration of competing interest

The authors declare that they have no known competing financial interests or personal relationships that could have appeared to influence the work reported in this paper.

Acknowledgements

We are grateful to Amicia Lee and an anonymous reviewer for detailed and very helpful comments.

References

Anderson, D.L., 1970. Petrology of the upper mantle. Mineral. Soc. Amer. Spec. Pap. 3, 85–93.

Berryman, J.G., 1980a. Long-wavelength propagation in composite elastic media I. Spherical inclusions. J. Acoust. Soc. Am. 68, 1809–1819.

Berryman, J.G., 1980b. Long-wavelength propagation in composite elastic media II. Ellipsoidal inclusions. J. Acoust. Soc. Am. 68, 1820–1831.

Berryman, J.G., 1995. Mixture theories for rock properties. In: Rock Physics and Phase Relations. A Handbook of Physical Constants. American Geophysical Union, pp. 205–228.

Carcione, J.M., 2014. Wave fields in real media. In: Theory and Numerical Simulation of Wave Propagation in Anisotropic, Anelastic, Porous and Electromagnetic Media, 3rd edition. Elsevier.

Carcione, J.M., Poletto, F., 2013. Seismic rheological model and reflection coefficients of the brittle-ductile transition. Pure Appl. Geophys. 170, 2021–2035.

Carcione, J.M., Helle, H.B., Gangi, A.F., 2006. Theory of borehole stability when drilling through salt formations. Geophysics 71, F31–F47.

Carcione, J.M., Helle, H.B., Avseth, P., 2011. Source-rock seismic-velocity models. Gassmann versus Backus, Geophysics 76, N37–N45.

Carcione, J.M., Poletto, F., Farina, B., Craglietto, A., 2014. Simulation of seismic waves at the brittle-ductile transition based on the Burgers model. Solid Earth 5, 1001–1010.

Carcione, J.M., Poletto, F., Farina, B., Craglietto, A., 2017. The Gassmann-Burgers model to simulate seismic waves at the Earth crust and mantle. Pure Appl. Geophys. 174, 849–863.

Carcione, J.M., Poletto, F., Farina, B., 2018a. The Burgers/squirt-flow seismic model of the crust and mantle. Phys. Earth Planet. Inter. 274, 14–22.

Carcione, J.M., Poletto, F., Farina, B., Bellezza, C., 2018b. 3D seismic modeling in geothermal reservoirs with a distribution of steam patch sizes, permeabilities and saturations, including ductility of the rock frame. Phys. Earth Planet. Inter. 279, 67–78.

Carcione, J.M., Wang, Z.-W., Ling, W., Salusti, E., Ba, J., Fu, L.-Y., 2018c. Simulation of wave propagation in linear thermoelastic media. Geophysics. https://doi.org/10.1190/geo2018-0448.1.

Ciz, R., Shapiro, S., 2007. Generalization of Gassmann equations for porous media saturated with a solid material. Geophysics 72, A75–A79 Erratum (vol. 74, 2009/01/01).

Corana, A., Marchesi, M., Martini, C., Ridella, S., 1987. Minimizing multimodal functions of continuous variables with the simulated annealing algorithm. ACM Trans. Math. Softw. 13, 262–280.

Engelder, T., 1993. Stress Regimes in the Lithosphere. Princeton University Press.

Farina, B., Poletto, F., Mendrinos, D., Carcione, J.M., Karytsas, C., 2019. Seismic properties in conductive and convective hot and super-hot geothermal systems. Geotehrmics 82, 16–33.

Finetti, I.R. (Ed.), 2005. CROP Project: Deep Seismic Exploration of the Central Mediterranean and Italy (Atlases in Geosciences). vol. 1 and 2 Elsevier.

Gangi, A.F., 1983. Transient and steady-state deformation of synthetic rocksalt. Tectonophysics 91, 137–156.

Goffe, W.L., Ferrier, G.D., Rogers, J., 1994. Global optimization of statistical functions with simulated annealing. J. Econ. 60 (1–2), 65–99.

Gurevich, B., Carcione, J.M., 2000. Gassmann modeling of acoustic properties of sand/clay mixtures. Pure Appl. Geophys. 157, 811–827.

Hammond, W.C., Humphreys, E.D., 2000. Upper mantle seismic wave attenuation: effects of realistic partial melt distribution. J. Geophs. Res. 105, 10987–10999.

Hashin, Z., Shtrikman, S., 1963. A variational approach to the theory of the elastic behaviour of multiphase materials. Journal of the Mechanics and Physics of Solids 11, 127–140.

Hegret, G., 1987. Stress assumption for underground excavation in the Canadian Shield. Int. J. Rock Memch. Min. Sci. Geomech. Abstr. 24, 95–97.

Henriques, J.P., de Figueiredo, J.J., Santos, L.K., Macedo, D.L., Coutinho, I., da Silva, C.B., Melo, A.L., Sousa, M., Azevedo, F.L., 2017. Experimental verification of effective anisotropic crack theories in variable crack aspect ratio medium. Geophys. Prosp. https://doi.org/10.1111/1365-2478.12544.

Hill, R., 1963. Elastic properties of reinforced solids: some theoretical principles. J. Mech. Phys. Solids 11, 357–372.

Hill, R., 1965. Self-consistent mechanics of composite materials. J. Mech. Phys. Solids 13, 213–222.

Jackson, I., 2015. Properties of rocks and minerals - physical origins of anelasticity & attenuation in rock. In: Schubert, Gerald (Ed.), Treatise on Geophysics, Second edition. Elsevier B.V, Amsterdam, Netherlands, pp. 539–571.

Jackson, I., Faul, H., Fitzgerald, J., Morris, S., 2006. Contrasting viscoelastic behaviour of melt-free and melt-bearing olivine: implications for the nature of grain-boundary sliding. Mater. Sci. Eng. A 442, 170–174.

Karato, S., Spetzler, H.A., 1990. Defect microdynamics and physical mechanisms of seismic wave attenuation and velocity dispersion in the Earth's mantle. Rev. Geophys. 28, 399–421.

Kerner, E.H., 1956. The elastic and thermo-elastic properties of composite media. Proc. Roy. Soc. London 69B, 808–813.

Kim, E., Kim, Y., Mainprice, D., 2019. GassDem: a MATLAB program for modeling the anisotropic seismic properties of porous medium using differential effective medium theory and Gassmann's poroelastic relationship. Comput. Geosci. 126, 131–141.

Kuster, G.T., Toksóz, M.N., 1974. Velocity and attenuation of seismic waves in two-phase media, I. Theoretical formulation. Geophysics 39, 587–606.

Lee, A.L., Walker, A.M., Lloyd, G.E., Torvela, T., 2017. Modeling the impact of melt on seismic properties during mountain building. Geochem. Geophys. Geosyst. 18, 1090–1110.

Mainardi, F., 2010. Fractional Calculus and Waves in Linear Viscoelasticity. Imperial College Press, London.

Man, C.-S., Huang, M., 2011. A simple explicit formula for the Voigt-Reuss-Hill average of elastic polycrystals with arbitrary crystal and texture symmetries. J. Elast. 105, 29–48.

Mavko, G.M., 1980. Velocity and attenuation in partially molten rocks. J. Geophys. Res. 85, 5173–5189.

Mavko, G.M., Nur, A., 1975. Melt squirt in the asthenosphere. J. Geophys. Res. 80, 1444–1448.

Mavko, G., Mukerji, T., Dvorkin, J., 2009. The Rock Physics Handbook. Cambridge Univ. Press.

McCarthy, C., Takei, Y., 2011. Anelasticity and viscosity of partially molten rock analogue: toward seismic detection of small quantities of melt. Geophys. Res. Lett. 38, L18306.

Nur, A., 1971. Viscous phase in rocks and the low-velocity zone. J. Geophys. Res. 76 (5), 1270–1277.

Pichler, Ch., Lackner, R., 2009. Upscaling of viscoelastic properties of highly-filled composites: investigation of matrix-inclusion-type morphologies with power-law viscoelastic material response. Composites Science and Technology 69, 2410–2420.

Picotti, S., Carcione, J.M., Ba, J., 2018. Rock-physics templates for seismic Q. Geophysics 84 (1), MR13–MR23.

Richard, T.G., 1975. The mechanical behavior of a solid microsphere filled composite. J. Composite Materials 108–113.

Rimas Vayšnis, J., 1968. Propagation of acoustic waves through a system undergoing phase transformations. J. Geophys. Res. 73 (24), 7675–7683.

Sato, H., Sacks, I.S., Murase, T., Muncill, G., Fukuyama, H., 1988. Attenuation of compressional waves in peridotite measured as a function of temperature at 200 MPa. Pure Appl. Geophys. 128, 433–447.

Schmeling, H., 1985. Numerical models on the influence of partial melt on elastic, anelastic and electric properties of rocks. Part I: elasticity and anelasticity. Physics a/the Earth and Planetary Interiors 41, 34–57.

Sun, Y.F., Goldberg, D., 1997a. Estimation of aspect-ratio changes with pressure from seismic velocities. In: Lovell, M.A., Harvey, P.K. (Eds.), Developments in Petrophysics. Geological Society Special Publication No. 122pp. 131–139.

Sun, Y.F., Goldberg, D., 1997b. Effects of Aspect Ratio on Wave Velocities in Fractured Rocks, SEG Expanded Abstract.

Takei, Y., 2000. Acoustic properties of partially molten media studied on a simple binary system with a controllable dihedral angle. J. Geophys. Res. 105, 16665–16682.

Takei, Y., 2017. Effects of partial melting on seismic velocity and attenuation: a new insight from experiments. Annu. Rev. Earth Planet. Sci. 45, 447–470.

Takeuchi, S., 1972. Variation of elasticity in water-saturated rocks near the melting temperature of ice. Contributions, Geophysical Institute, Kyoto University, No. 12 (1972), 157–176.

Villeneuve, N., Neuville, D.R., Boivin, P., Bachèlery, P., Richet, P., 2008. Magma crystallization and viscosity: a study of molten basalts from the Piton de la Fournaise volcano (La Réunion island). Chem. Geol. 256, 242–251.

Waff, U.S., Bulau, J.R., 1979. Equilibrium fluid distribution in an ultramafic partial melt under hydrostatic stress conditions. J. Geophys. Res. 84, 6109–6114.

Walsh, J.B., 1968. Attenuation in partially melted material. J. Geophys. Res. 73 (6), 2209–2216.

Walsh, J.B., 1969. New analysis of attenuation in partially melted rock. J. Geophys. Res. 74, 4333–4337.

Wu, T.T., 1966. The effect of inclusion shape on the elastic moduli of a two-phase material. Int. J. Solids Struct. 2, 1–8.

Xu, S., Payne, M.A., 2009. Modeling Elastic Properties in Carbonate Rocks, the Leading Edge. (May issue).

Yang, Z.-Q., He, T., Zou, C.-C., 2017. Shales in the Qiongzhusi and Wufeng–Longmaxi formations: a rock-physics model and analysis of the effective pore aspect ratio. Appl. Geophys. 14, 325–336.

Zhang, H., Srolovitz, D.J., Douglas, J.F., Warren, J.A., 2009. Grain boundaries exhibit the dynamics of glass-forming liquids. PNAS 106 (19), 7735–7740 May 12.